

# On the Brightening Propagation of Post-Flare Loops Observed by TRACE

Leping Li and Jun Zhang

*National Astronomical Observatories, Chinese Academy of Sciences, Beijing 100012, China; lepingli;zjun@ourstar.bao.ac.cn*

## ABSTRACT

Examining flare data observed by TRACE satellite from May 1998 to December 2006, we choose 190 (151 M-class and 39 X-class) flare events which display post-flare loops (PFLs), observed by 171 Å and 195 Å wavelengths. 124 of the 190 events exhibit flare ribbons (FRs), observed by 1600 Å images. We investigate the propagation of the brightening of these PFLs along the neutral lines and the separation of the FRs perpendicular to the neutral lines. Observations indicate that the footpoints of the initial brightening PFLs are always associated with the change of the photospheric magnetic fields. In most of the cases, the length of the FRs ranges from 20 Mm to 170 Mm. The propagating duration of the brightening is from 10 minutes to 60 minutes, and from 10 minutes to 70 minutes for the separating duration of the FRs. The velocities of the propagation and the separation range from 3 km s<sup>-1</sup> to 39 km s<sup>-1</sup> and 3 km s<sup>-1</sup> to 15 km s<sup>-1</sup>, respectively. Both of the propagating velocities and the separating velocities are associated with the flare strength and the length of the FRs. It appears that the propagation and the separation are dynamically coupled, that is the greater the propagating velocity is, the faster the separation is. Furthermore, a greater propagating velocity corresponds to a greater deceleration (or acceleration). These PFLs display three types of propagating patterns. Type I propagation, which possesses about half of all the events, is that the brightening begins at the middle part of a set of PFLs, and propagates bi-directionally towards its both ends. Type II, possessing 30%, is that the brightening firstly appears at one end of a set of PFLs, then propagates to the other end. The remnant belongs to Type III propagation which displays that the initial brightening takes place at two (or more than two) positions on two (or more than two) sets of PFLs, and each brightening propagates bi-directionally along the neutral line. These three types of propagating patterns can be explained by a three-dimensional magnetic reconnection model.

*Subject headings:* Sun: flares —Sun: corona—Sun: UV radiation—Sun: magnetic fields

## 1. INTRODUCTION

Flares are one of the most spectacular phenomena in solar physics. They are sudden brightening in the solar atmosphere, and consist of a number of components including loops, ribbons, arches, remote patches, surges, erupting filaments, and other expanding coronal features (Martin 1989). They have been studied morphologically from direct images (e.g. Krucker et al. 2000; Fletcher et al. 2001; Kundu et al. 2001) and spectroscopically from spectrograms (e.g. Moore 1976; Cowan et al. 1973; Acton et al. 1985; Cully et al. 1997; Grigis et al. 2005b) at different wavelength regions. Like most dynamic phenomena on the solar surface, the occurrence of solar flares is closely related to the presence and evolution of solar magnetic fields, especially the complicated, non-potential magnetic configuration (Rust 1972; Patterson & Zirin 1981; Moore et al. 1984). Flares can be caused by rotating sunspot (Brown et al. 2003; Tian et al. 2006; Zhang et al. 2007), magnetic flux emergence (Ishii et al. 1998; Wang et al. 2004; Li et al. 2007), magnetic flux cancellation (Livi et al. 1989; Wang et al. 1992, 1993; Zhang et al. 2001a,b, 2002), magnetic shear (Kusano et al. 2004; Wang et al. 2006; Ji et al. 2006; Su et al. 2007), and so on.

The chromospheric flare (e.g. Fang et al. 2000; Falchi et al. 2002; Cheng et al. 2006; Hudson 2007) is easier to be observed, especially with the help of an  $H\alpha$  filter. Larger flares often occur right after the sudden disappearance of a filament (Kuperus et al. 1981; Ding et al. 2003; Sterling et al. 2005; Jiang et al. 2006a,b; Chifor et al. 2007). In this case, the flare generally has the form of two flare ribbons (FRs) which lie on both sides of the location of the former filament. During flare decay phase, the FRs move apart. The separation of these FRs has been used to estimate the electric field in the reconnecting current sheet (e.g. Qiu et al. 2002; Asai et al. 2004b) and also the coronal magnetic field strength and the reconnection rate (e.g. Isobe et al. 2002b, 2005). Many authors have observed the parallel and antiparallel movements of the FRs along the arcade (Hoyng et al. 1981; Takakura et al. 1983; Fletcher & Hudson 2002; Liu et al. 2004; Qiu et al. 2004; Siarkowski & Falewicz 2004).

Accompanying the FRs is a system of post-flare loops (PFLs) which initially appears at low altitude and then moves upward into the corona in consort with the motion of the ribbons (Moore et al. 1980). A classical description of the PFLs, as seen in  $H\alpha$  images, was first given by Bruzek (1964) who noted that the ribbons essentially lie at the footpoints of the loop system, which forms a series of arcades (Lin et al. 2003). These arcades are also frequently seen in the X-ray images recorded by Soft X-ray Telescope (SXT) (Tsuneta et al. 1991) aboard Yohkoh (Ogawara et al. 1991), in the extreme ultraviolet (EUV) images from EIT (Extrmeme-ultraviolet Imaging Telescope, Delaboudinière et al. 1995) aboard the Solar and Heliospheric Observatory (SOHO) (Domingo et al. 1995), and also in the EUV

images from Transition Region and Coronal Explorer (TRACE) (Handy et al. 1999). The formation of transient large-scale PFLs or post-eruptive arcades (PEAs) has been widely studied (e.g. Carmichael 1964; Sturrock 1966; Hirayama 1974; Kopp & Pneuman 1976; Cargill et al. 1983; Webb & Hundhausen 1987; Svestka et al. 1997; Tripathi et al. 2004; Tripathi 2005, 2006b). Hudson et al. (1998), Sterling et al. (2000) and Tripathi (2006b) studied a set of individual events about the relationship between PFLs and Coronal Mass Ejections (CMEs). The propagation of the loop formations along the neutral line, together with the separation of the FRs perpendicular to the neutral line was reported by Isobe et al. (2002a). Grigis & Benz (2005a) found a RHESSI observation showing that the hard X-ray (HXR) sources do not show the separation from the neutral line, but instead they move along the neutral line (see also Goff et al. 2007). Tripathi et al. (2006a) investigated the relationship between the brightening propagation of the PEAs and the erupting filament/prominence. They reported two types of propagation of the brightening, and the propagating direction was consistent with the erupting direction of the filaments.

Due to the extremely low density and high temperature of the corona, measurements of the magnetic field are restricted to lower layers of the solar atmosphere. For this reason, extrapolation techniques, which attempt to reconstruct the coronal field from measured boundary values in the photosphere (or low chromosphere), are the prime tool for quantitative investigations of the coronal magnetic field (Valori et al. 2005). Some authors used the methods of extrapolation to study the evolution of flare loops in active region (e.g. Yan et al. 1995; Wang et al. 2001; Wiegmann et al. 2005; Amari et al. 2006; Zhao et al. 2008).

Magnetic reconnection of solar coronal loops is considered to be the main process that causes solar flares and possibly coronal heating. It is widely believed to be a mechanism of magnetic energy release (see reviews by Shibata 1999; Martens 2003), and plays an important role in various explosive phenomena in astrophysical, space, and laboratory plasmas (Biskamp 1993; Tajima & Shibata 1997; Priest & Forbes 2000). The evidence of magnetic reconnection found by space observations includes the cusp-shaped PFLs (Tsuneta et al. 1992), the loop-top hard X-ray source (Masuda et al. 1994), the reconnection inflow (Yokoyama & Shibata 2001; Lin 2005), downflows above PFLs (McKenzie & Hudson 1999; Innes et al. 2003; Asai et al. 2004a), plasmoid ejections (Shibata et al. 1995; Ohyama & Shibata 1997; Ohyama & Shitaba 1998), etc. Two-dimensional (e.g. De Young et al. 1971; Winglee et al. 1991; Hu et al. 1995; Forbes et al. 1995; Yokoyama & Shibata 1998; Zhang et al. 2006) and three-dimensional simulations (e.g. Wu et al. 1992; Magara et al. 1999; Miyagoshi et al. 2004; Aulanier et al. 2006; Birn et al. 2006) are widely used to study the magnetic reconnection in process of flares and CMEs.

The magnetic reconnection model proposed by Carmichael (1964), Sturrock (1966),

Hirayama (1974) and Kopp & Pneuman (1976) (the CSHKP model) suggests that magnetic field lines successively reconnect in the corona. This model explains several well-known features of solar flares, such as the growth of flares loops with a cusp-shaped structure and the formation of the  $H\alpha$  two-ribbon structures at their footpoints. In recent decades, this model has been further extended (e.g. Pneuman 1981; Priest & Forbes 1990, 2000, 2002; Moore & Roumeliotis 1992; Moore et al. 2001; Shibata 1999; Yokoyama & Shibata 2001; Lin et al. 2000; Lin 2004).

In this paper, we mainly study the dynamic evolution of a larger sample of flare events, including the propagation of the PFLs along the neutral lines and the separation of the FRs away from the neutral lines. This investigation will provide some information of 3-dimensional magnetic reconnection in the process of flare. The criteria for the data selection and the methods of the data analysis are described in section 2. In section 3, we summarize our statistical results. Conclusions and brief discussion are shown in section 4.

## 2. DATA AND OBSERVATIONS

We checked all the 75 X-class and 509 M-class flare events<sup>1</sup> observed by TRACE from May 1998 to December 2006. 39 X-class and 151 M-class flare events which display PFLs are chosen as our sample (see Table 1). The TRACE mission explores the dynamics and evolution of the solar atmosphere from the photosphere to the corona with high spatial and temporal resolution (Handy et al. 1999). It observes the photosphere (white-light, WL), the transition region (1216, 1550, and 1600 Å) and the 1-2 MK corona (171, 195, and 284 Å). In this work, we mainly use the 171 and 195 Å images to study the propagation of the brightening of the PFLs, and the 1600 Å observations to the separation of the FRs. We also use TRACE WL observations and magnetic field observations of SOHO/MDI (Scherrer et al. 1995) to investigate the variation of the source region of these flare events.

### 2.1. Methods

In order to study the dynamic evolution of the larger sample of flare events quantitatively, we determine a set of parameters to describe the evolution of the PFLs and the FRs for each event in our sample. These parameters include the propagating duration ( $PD$ ), propagating velocity ( $V_p$ ) and acceleration ( $a_p$ ) of the PFLs, the separating duration ( $SD$ )

---

<sup>1</sup>[http://hea-www.harvard.edu/trace/flare\\_catalog/index.html](http://hea-www.harvard.edu/trace/flare_catalog/index.html)

and separating velocity ( $V_s$ ) of the FRs, the length ( $Len$ ) of the FRs at the maximum of the flare, the flare class ( $FC$ ) and the flare duration ( $FD$ ). Because some events in the sample are not completely observed, we can not get all the parameters simultaneously for all the cases. Among the 190 flare events, 183 display clear evolution of the PFLs observed by TRACE 171 and 195 Å images, so we can measure the three parameters  $V_p$ ,  $a_p$  and  $PD$ . TRACE 1600 Å observations can clearly detect the FRs. In our sample, 124 events are also observed by TRACE 1600 Å wavelength, so we measure the parameter  $Len$  for these events. 101 of the 124 events show clear kinetics of the FRs, we measure  $V_s$  and  $SD$  for these cases. Table 2 lists the measured events of these parameters.

In order to illustrate how to measure these parameters, we show a flare event observed on the disk at the heliographic position S05 W54 on 2001 March 20 in Fig. 1. Figure 1a shows the initial brightening of PFLs at 02:41 UT.  $L_{21}$  and  $L_{22}$  in Fig. 1b represent the distance of the propagation of the PFLs towards southeast along different FRs from 02:41 UT to 03:16 UT, as well as  $L_{11}$  and  $L_{12}$ , towards northwest. The total value of these four distance represents the distance of the propagation ( $L_p$ ) of the PFLs from 02:41 UT to 03:16 UT:

$$L_p = L_{11} + L_{12} + L_{21} + L_{22} . \quad (1)$$

$L_{31}$  and  $L_{32}$  in Fig. 1c show the distance of the propagation of the PFLs toward southeast from 02:41 UT to 03:52 UT, as well as  $L_{41}$  and  $L_{42}$ , towards northwest. The distance of the propagation of PFLs from 02:41 UT to 03:52 UT is:

$$L_p = L_{31} + L_{32} + L_{41} + L_{42} . \quad (2)$$

By using the method shown above, we obtain a series of propagating distance of the PFLs with time, and a series of propagating velocities is derived. Both the initial propagating time ( $t_{pi}$ ) and the end propagating time ( $t_{pe}$ ) of the brightening of the PFLs are determined from the series of velocities. We define  $t_{pe}$  to be the time when the propagation velocity drops to 1/e of the peak value. The parameter  $PD$  of the PFLs is the duration of  $t_{pi}$  and  $t_{pe}$ . The distance versus time plot for the propagation of the PFLs between  $t_{pi}$  and  $t_{pe}$  for the event showed in Fig. 1 is indicated in Fig. 2. We use a linear polynomial fit to the data points to get the parameters  $V_p$ , and second order polynomial fit for  $a_p$ . Similar to the determination of  $t_{pi}$  and  $t_{pe}$ , the initial separating time ( $t_{si}$ ) and the end separating time ( $t_{se}$ ) of the FRs are obtained from 1600 Å observations. The parameter  $SD$  is the duration from  $t_{si}$  to  $t_{se}$ . Figures 1d-1f are series of 1600 Å images observed by TRACE.  $L_{51}$  and  $L_{52}$  in Fig. 1f represent the distance of the separation of the FRs from 02:25 to 03:27 UT towards northeast and southwest, respectively. The distance of the separation ( $L_s$ ) of the FRs is

$$L_s = L_{51} + L_{52} . \quad (3)$$

We got the parameter  $V_s$  using the similar method as to get  $V_p$ . The length of the FRs is measured from 1600 Å image (see Fig. 1e) while the FRs are well developed.  $L_{61}$  and  $L_{62}$  represent the length of two FRs, respectively. We get  $Len$  by using

$$Len = \frac{L_{61} + L_{62}}{2}. \quad (4)$$

The projection effects are corrected using trigonometric function when we got the parameters  $V_p$ ,  $a_p$ ,  $V_s$  and  $Len$ .

The parameter  $FC$ , the peak X-ray flux of the associated flare, is recorded by GOES-10 soft X-ray 1-8 Å flux intensity, and  $FD$ , the duration between the beginning time and the ending time of the flares, by Solar-Geophysical Data. While studying the evolution of the PFLs of these events, we find that the PFLs display three types of propagating patterns. Type I is that the brightening begins at the middle part of a set of PFLs, and then propagates bi-directionally towards its both ends. Type II shows that the brightening firstly appears in one end of a set of PFLs, then propagates to the other end. There are two (or more than two) initial brightening involved in Type III propagation, each brightening takes place in the middle of a set of PFLs, then propagates bi-directionally. The following are three examples of flare events which are displayed to describe the three types of propagation.

## 2.2. M 9.8 Flare on 2005 September 17

Type I propagation is characterized by an M 9.8 flare event occurred at the heliographic position S11 W51 on 2005 September 17. We show the time sequence of 171 Å images in the top panels of Fig. 3. The brightening of the PFLs is firstly seen at 06:04 UT, and the outer edges of the PFLs are outlined as dotted curves in Fig. 3a. The propagation of the PFLs ended at 06:24 UT (see Figure 3c). From these panels, we notice that the initial brightening of this event occurs at the middle part of a set of PFLs, then propagates bi-directionally towards its both ends (see white arrows in Fig. 3c).

We examine the evolution of photospheric magnetic field and the change of continuum intensity by using the observations of SOHO/MDI and TRACE WL, respectively. Figure 3d is the magnetogram before the flare, as well as Fig. 3e, after the flare. Figure 3f displays the difference image of these two magnetograms. The regions in white brackets show the change of photospheric magnetic field, and the variation of unsigned magnetic flux is about  $3 \times 10^{20}$  Mx. The TRACE WL images before and after the flare are presented in Figs. 3g and 3h, respectively. We show their difference image in Fig. 3i, and find the change of the continuum intensity (denoted by white brackets). Comparing Figs. 3f and 3i with Figs. 3a and 3c, we note that the regions showing obvious changes of photospheric magnetic field and continuum

intensity are associated with the initial brightening of the PFLs (see the brackets in Figs. 3*a* and 3*c*). In other words, the initial brightening is related to the magnetic variation on the photosphere.

### 2.3. M 2.0 Flare on 1999 January 18

The M 2.0 flare event on 1999 January 18, which occurred at the heliographic position N19 E03, is used to describe Type II propagation. Figures 4*a* and 4*c* are the TRACE 171 Å images showing the beginning and the ending propagation of the brightening of the PFLs. Figure 4*b* is an image during the propagation. It appears that the initial brightening occurs at the southern end of a set of PFLs, and then propagates towards northeastern end (see the white arrow in Fig. 4*c*).

As this event was not observed by SOHO/MDI, we use TRACE WL images to study the change of the continuum intensity (the bottom panels of Fig. 4) which are relevant to this event. Figures 4*d* and 4*e* are the observations before and after the flare, and Fig. 4*f* is their difference image. The regions inside the square brackets in Fig. 4*a* show the footpoints of the initial brightening of the PFLs. We overlay these square brackets on Fig. 4*f*, and find that the initial brightening of the PFLs is associated with the change of the continuum intensity.

### 2.4. M 1.5 Flare on 2002 October 25

The M 1.5 flare event on 2002 October 25 occurred at the heliographic position N28 W11. This event is employed to display Type III propagation. Figure 5*a* shows the initial brightening of the PFLs in the southwest of the FRs, with dotted curves outlining the outer edge of the PFLs. Then this brightening propagates towards northeast and southwest (see the black arrows showed in Fig. 5*c*). Figure 5*b* presents the brightening of another set of PFLs (marked by the dashed line). This brightening also propagates towards northeast and southwest (see the white arrows in Fig. 5*c*). From these panels, we notice that the PFLs are consist of two sets of independent brightening loops in different places in the active region, then each brightening propagates bi-directionally towards its both sides.

Figures 5*d* and 5*e* are longitudinal magnetograms before and after the flare observed by SOHO/MDI, respectively. Figure 5*f* shows their difference signal. We mark the regions of the PFL footpoints as brackets in Figs. 5*a*-5*b* and overlay these regions on the difference magnetogram (see Fig. 5*f*). It indicates that the regions of the initial brightening are

associated with the change of the photospheric magnetic field, as presented in section 2.2.

### 3. STATISTICAL RESULTS

In this work, eight parameters ( $PD$ ,  $V_p$  and  $a_p$  of PFLs,  $SD$ ,  $V_s$  and  $Len$  of FRs,  $FC$  and  $FD$ ) are considered to characterize the kinematics of the PFLs and the FRs, and listed in Table 2.

By examining the TRACE observations of all the flare events, we have determined  $PD$  of 183 events and  $SD$  of 101 events. Figure 6a shows the distribution of  $PD$  (solid lines) and  $SD$  (dotted lines).  $PD$  ranges from 10 to 60 minutes in nearly 90% of the cases, with the peak of the distribution lying close to 25 minutes. The average value of all the  $PD$ s is 33 minutes. Similarly, almost 90% of the  $SD$ s range from 10 to 70 minutes, with average duration of 38 minutes. Besides  $PD$  and  $SD$ , we have also exhibited the distribution of  $V_p$  (solid lines) and  $V_s$  (dotted lines) in Fig. 6b. Most of the  $V_p$ s range from 3 to 33 km s<sup>-1</sup>, and the average velocity is 17.9 km s<sup>-1</sup>. It indicates that 76% of the  $V_s$ s range from 3 to 15 km s<sup>-1</sup>, with the average value of 7.2 km s<sup>-1</sup>.

In order to explore the physical connection of these parameters, we study the one-to-one correspondence among them. It appears that  $FD$  is associated with  $PD$  and  $SD$ , and the longer the  $FD$  is, the longer the  $PD$  and the  $SD$  are, as displayed in Fig. 7. The  $Len$  of the FRs, which ranges mainly from 20 to 170 Mm and may represent the length of the current sheet along the neutral line, is associated with  $FC$  and weakly associated with  $FD$  (see Fig. 8). It looks like that more powerful flares correspond to longer FRs.  $V_p$  and  $V_s$  are two important parameters, as they represent the kinetics of the propagation of the PFLs and the separation of the FRs. Figure 9 shows the correspondence of  $V_p$  and  $V_s$  with some relevant parameters. Generally, both of  $V_p$  and  $V_s$  increase as the flare becomes more powerful (see Figs. 9a and 9c). Figures 9b and 9d show the relationship between the velocity and  $Len$  of the FRs, separately for  $V_p$  (Fig. 9b), and  $V_s$  (Fig. 9d). It displays that both  $V_p$  and  $V_s$  increase from several km s<sup>-1</sup> to tens of km s<sup>-1</sup>, as  $Len$  increases from tens of Mm to hundreds of Mm.

The separation of the FRs, considered to be the representation of continuing magnetic reconnection and upwards moving reconnection sites, has been well studied. The propagation of the PFLs, which may reflect the signature of successive magnetic reconnection along the neutral line, is rarely taken into account. In our statistical results, we notice that  $V_s$  is associated with  $V_p$  (see Fig. 10a), that is  $V_s$  increases as  $V_p$  increases. Besides the velocity,  $a_p$  is also an important parameter to study the evolution of the PFLs. Figure 10b shows the



relationship between  $a_p$  and  $V_p$ . The diamonds represent the positive accelerations of the brightening propagation, as well as the asterisks, decelerations. Among these 183 events, 135 are decelerated, possessing 74%, and 48 accelerated, occupying 26%. There is also a trend that the greater the  $V_p$  is, the larger the deceleration (or acceleration) is.

In this study, we classify the propagation of the PFLs into three types. The information of these three types of propagation is showed in Table 3. It appears that the events displaying Type I propagation are almost half of all the events.

#### 4. CONCLUSIONS AND DISCUSSION

We have studied the evolution of the PFLs and the FRs of the 190 flare events, and obtained the following results.

1. Both of  $PD$  and  $SD$  are associated with  $FD$ . The longer the  $FD$  is, the longer the  $PD$  and the  $SD$  are. The length of the FRs mainly ranges from 20 to 170 Mm. It is associated with  $FC$ , but weakly associated with  $FD$ . It increases as  $FC$  ( $FD$ ) increases.

2.  $V_p$  ranges mainly from 3 km s<sup>-1</sup> to 33 km s<sup>-1</sup>, and  $V_s$ , from 3 km s<sup>-1</sup> to 15 km s<sup>-1</sup> in 76% of the cases.  $V_p$  and  $V_s$  are dynamically coupled,  $V_p$  increases as  $V_s$  increases. Both of  $V_p$  and  $V_s$  are positively correlated with  $FC$  and  $Len$  of the FRs. The brightening of the PFLs do not evenly propagate, 74% of the PFL events are decelerated, and 26%, accelerated.

3. There are three types of propagation of the PFLs. Type I, possessing 49.5% of all the events, is that the brightening begins at the middle part of a set of PFLs, and then propagates bi-directionally towards its both ends. Type II, in possession of 30%, displays that the brightening firstly appears in one end of a set of PFLs, then propagates to the other end. Type III, occupying 20.5%, shows that the initial brightening takes place at two (or more than two) positions on two (or more than two) sets of PFLs, and each brightening propagates bi-directionally.

The main error source of our measurement of the velocities ( $V_p$  and  $V_s$ ) is due to the uncertainty of the outer edges. In our study, two pixels error has been used. As the average  $PD$  ( $SD$ ) is 33 (38) minutes, the error of  $V_p$  ( $V_s$ ) is 0.4 (0.3) km s<sup>-1</sup>, which is much less than the velocities showed in Table 1. So the values of these velocities are reliable.

Several authors have paid attention to the propagation of the PFLs. Isobe et al. (2002a) reported that  $V_p$  is about 3-30 km s<sup>-1</sup> by using the data from Yohkoh/SXT (Tsuneta et al. 1991), and 50-150 km s<sup>-1</sup> in Grigis & Benz (2005a) from RHESSI observations. Based on the SOHO/EIT observations, Tripathi et al. (2006a) studied several flare events relevant

to long filament eruptions. They presented that  $V_p$  of the PEAs ranges from 20 to 111 km s<sup>-1</sup>. In this paper, we show that  $V_p$  is mainly from 3 to 33 km s<sup>-1</sup>, which is consistent with Isobe et al. (2002a), but somewhat smaller than that of Tripathi et al. (2006a). The velocity difference between ours and Tripathi et al. may result from two aspects. The first aspect is the sample. Our sample contains hundreds of cases. The second is the datum source. We employ the TRACE data which have higher spatial (1'') and temporal (1 minute) resolution.  $V_s$  of the FRs have been intensively studied, but the value are varied distinctly, e.g. 20-100 km s<sup>-1</sup> in Qiu et al. (2002), 0-85 km s<sup>-1</sup> in Asai et al. (2004b, 2006) and 20-70 km s<sup>-1</sup> in Temmer et al. (2007). By employing the TRACE 1600 Å observations, Isobe et al. (2005) obtained  $V_s$  of 6.7-12 km s<sup>-1</sup> near the impulsive phase of the flares. Our results about  $V_s$  (3-15 km s<sup>-1</sup>) are well in agreement with that of Isobe et al. (2005).

It is basically accepted that the separation of the FRs and the propagation of the PFLs can be considered the signature of the successive magnetic reconnection along different directions.  $SD$  represents the duration of the magnetic reconnection where the reconnection points move upward, and  $PD$ , along the neutral lines. Both  $SD$  and  $FD$  determine the duration of flares. That is the reason why both  $SD$  and  $PD$  are associated with  $FD$  (see Figs. 7a-b). Lots of researchers have employed  $V_s$  to estimate the reconnection rate, they derived that the reconnection rate is very sensitive to  $V_s$  (e.g. Isobe et al. 2002b, 2005). Investigation of the propagation of the PFLs and the separation of the FRs simultaneously will provide us with 3-dimensional picture of magnetic reconnection in the process of flares. In our study, we find that  $V_p$  of the PFLs is associated with  $V_s$  of the FRs (see Fig. 10a). This indicates that the separation of the FRs and the propagation of the PFLs are dynamical coupled. Our results show that both  $V_s$  of the FRs and  $V_p$  of the PFLs are associated with  $FC$  (see Figs. 9a and 9c). As  $FC$  represents the maximum energy release rate of the flares, this implies that  $V_s$  and  $V_p$  may also reflect the magnetic reconnection rate.  $Len$  of the FRs may be the length of the current sheet along the neutral line. Both  $V_s$  of the FRs and  $V_p$  of the PFLs are associated with  $Len$  of the FRs (see Figs. 9b and 9d). This may result from the magnetic configuration of the source region of the flare. Tripathi et al. (2006a) have suggested that the longer the FRs is, the less magnetically complex the flare region is. We speculate that the brightening of the PFLs propagates easily in a simple magnetic configuration, and so do the FRs separate. All the parameters and the relationships between these parameters we discussed here will help us to better understand 3-dimensional magnetic reconnection, and provide an observational character for theoretical study and simulation of 3-dimensional magnetic reconnection.

By investigating 17 events, Tripathi et al. (2006a) found two types of propagation of the brightening of the PEAs associated with asymmetric eruptions and symmetric eruptions of filaments, respectively. We have studied a much larger sample with higher spatial

and temporal resolution observations, and found three types of propagation of the PFLs. Type I and Type II propagation are similar to those two types of propagations reported by Tripathi et al. (2006a). Type III propagation indicates that sometimes two or more than two sets of PFLs are involved in a flare event. All the three types of the propagation of the PFLs may be explained by schematic diagrams shown in Fig. 11 (see also Shiota et al. 2005; Tripathi et al. 2006a). Figure 11*a* shows the explanation of Type I propagation. The X-point of the magnetic reconnection site occurs over the middle part of a set of loops (marked by *Reconnection*), then continuing magnetic reconnection occurs bi-directionally, thus results in the brightening of the PFLs appearing in the middle of the set of loops and propagating towards two opposite directions (see the grey thick arrows) as expected from the standard model. The white hollow arrows represent the separating direction of the FRs. Figure 11*b* illustrates that the magnetic reconnection site occurs over one end of a set of loops (mark by *Reconnection*), then the magnetic reconnection develops continuously towards the other end (see the black thick arrow). This mechanism can be employed to explain the observations of Type II propagation that the brightening of the PFLs occurs at one end of a set of PFLs and propagates from one end to the other one. Type III propagation displays a complex evolution pattern of the PFLs. We suggest that there are two (or more than two) magnetic reconnection sites (see Fig. 11*c*) which locate in two (or more than two) magnetic flux system. After the magnetic reconnection occurs, each of the brightening of the PFLs propagates bi-directionally along the neutral lines (see the black thick arrows). We check the MDI magnetograms and the TRACE WL observations of these events (e.g. see the examples displayed in Figs. 3-5), and find that the magnetic activity are clearly seen at the footpoints of the initial brightening of the PFLs. According to the observations of these three types of propagation, we propose that all the propagation of the PFLs are caused by magnetic reconnection. There is only one set of magnetic flux system involved in Type I and Type II propagation. The only difference of these two types of propagation is the position of the magnetic reconnection site. There are two or more than two sets of PFLs heated in the process of flare in Type III propagation. So the different appearance of these three types of the propagating PFLs may be determined by two effects. One is the different position of the magnetic reconnection site, the other is the different magnetic configuration of the source region of the flare.

Further studies using the data observed by Solar Terrestrial Relations Observatory (STEREO) will give us a more clear three-dimensional stereoscopic pictures about the evolution of the PFLs. Vector magnetograms (e.g. from Hinode) with higher spatial and temporal resolution are likely to uncover the magnetic configuration in detail. Moreover, complex three-dimensional simulation will be required to understand the dynamic behavior of the PFLs and the FRs.

The authors are indebted to the TRACE and SOHO/MDI teams for providing the data. The work is supported by the National Natural Science Foundations of China (G10703007, 10573025, 10603008, 40674081, and 10733020), the CAS Project KJCX2-YW-T04, and the National Basic Research Program of China under grant G2006CB806303.

## REFERENCES

- Acton, L. W., Bruner, M. E., Brown, W. A., et al. 1985, *ApJ*, 291, 865
- Amari, T., Aly, J. J., Mikic, Z., & Linker, J. 2006, *ApJ*, 671, L189
- Asai, A., Yokoyama, T., Shimojo, M., & Shibata, K. 2004a, *ApJ*, 605, L77
- Asai, A., Yokoyama, T., Shimojo, M., et al. 2004b, *ApJ*, 611, 557
- Asai, A., Yokoyama, T., Shimojo, M., Masuda, S., & Shibata, K. 2006, *J. Astrophys. Astr.*, 27, 167
- Aulanier, G., Pariat, E., Démoulin, P., & Devore, C.R. 2006, *Sol. Phys.*, 238, 347
- Birn, J., Forbes, T. G., & Hesse, M. 2006, *ApJ*, 645, 742
- Biskamp, D. 1993, *Nonlinear Magnetohydrodynamics* (cambridge: Cambridge Univ. Press)
- Brown, D. S., Nightingale, R. W., Alexander, D., et al. 2003, *Sol. Phys.*, 216, 79
- Bruzek, A. 1964, In: *AAS-NASA Symp. on Physics of Solar Flares*, 301
- Cargill, P. J., & Priest, E. R. 1983, *ApJ*, 266, 383
- Carmichael, H. 1985, in *The Physics of Solar Flares*, ed. W.N.Hess (NASA SP-50; Washington, DC: NASA), 451
- Cheng, J. X., Ding, M. D., & Li, J. P. 2006, *ApJ*, 653, 733
- Chifor, C., Tripathi, D., Mason, H. E., & Dennis, B. R. 2007, *A&A*, 472, 967
- Cowan, R. D., & Widing, K. G. 1973, *ApJ*, 180, 285
- Cully, S. L., Fisher, G. H., Hawley, S. L., & Simon, T., 1997, *ApJ*, 491, 910
- Delaboudinière, J.-P., Artzner, G. E., Brunaud, J., et al. 1995, *Sol. Phys.*, 162, 291
- Domingo, V., Fleck, B., & Poland, A. I. 1995, *Sol. Phys.*, 162, 1

- Ding, M. D., Chen, Q. R., Li, J. P., & Chen, P. F. 2003, *ApJ*, 598, 683
- De Young, D. S., & Hundhausen, A. J. 1971, *JGR*, 76, 2245
- Falchi, A., & Mauas, P. J. D. 2002, *A&A*, 387, 678
- Fang, C., Hénoux, J.-C., & Ding, M. D. 2000, *A&A*, 360, 702
- Fletcher, L., Metcalf, T. R., Alexander, D., Brown, D. S., & Ryder, L. A., 2001, *ApJ*, 554, 451
- Fletcher, L., & Hudson, H. S. 2002, *Sol. Phys.*, 210, 307
- Forbes, T. G., & Priest, E. R. 1995, *ApJ*, 446, 377
- Goff, C. P., van Driel-Gesztelyi, L., Démoulin, P., et al. 2007, *Sol. Phys.*, 187, 229
- Grigis, P. C., & Benz, A. O. 2005, *ApJ*, 625, L143
- Grigis, P. C., & Benz, A. O. 2005, *A&A*, 434, 1173
- Handy, B. N., Acton, L. W., Kankelborg, C. C., et al., 1999, *Sol. Phys.*, 187, 229
- Hirayama, T. 1974, *Sol. Phys.*, 133, 357
- Hoyng, P., Duijveman, A., Machado, M. E., et al. 1981, *ApJ*, 246, L155
- Hu, Y. Q., Li, X., & Ai, G. X. 1995, *ApJ*, 451, 943
- Hudson, H. S., Lemen, J. R., St. Cyr, O. C., Sterling, A. C., & Webb, D. F. 1998, *Geophys. Res. Lett.*, 25, 2481
- Hudson, H. S. 2007, *ASPC*, 368, 365
- Innes, D. E., McKenzie, D. E., & Wang, T. 2003, *Sol. Phys.*, 217, 247
- Ishii, T. T., Kurokawa, H. & Takeuchi, T. T. 1998, *ApJ*, 499, 898
- Isobe, H., Shibata, K., & Machida, S. 2002a, *Geophys. Res. Lett.*, 29, 10
- Isobe, H., Yokoyama, T., Shimojo, M., et al. 2002b, *ApJ*, 566, 528
- Isobe, H., Takasaki, H., & Shibata, K. 2005, *ApJ*, 632, 118
- Ji, H. S., Huang, G. L., Wang, H. M., et al. 2006, *ApJ*, 636, L173
- Jiang, Y. C., Li, L. P., & Yang, L. H. 2006a, *Chin. J. Astron. Astrophys.*, 6, 345

- Jiang, Y. C., Li, L. P., Zhao, S. Q., Chen, H. D., & Ma, S. L. 2006b, *NewA*, 11, 612
- Jing, J., Qiu, J., Lin, J., Qu, M., Xu, Y., & Wang, H. M. 2005, *ApJ*, 620, 1085
- Kopp, R. A., & Pneuman, G. W. 1976, *Sol. Phys.*, 50, 85
- Krucker, S., & Benz, A. O. 2000, *Sol. Phys.*, 191, 341
- Kundu, M. R., Nindos, A., White, S. M., & Grechnev, V. V. 2001, *ApJ*, 557, 880
- Kuperus, M., & van Tend, W. 1981, *Sol. Phys.*, 71, 125
- Kusano, K., Maeshiro, T., Yokoyama, T., & Sakurai, T. 2004, *ApJ*, 610, 537
- Li, H., Schmieder, B., Song, M. T., & Bommier, V. 2007, *A&A*, 475, 1081L
- Lin, J., & Forbes, T. G. 2000, *J. Geophys. Res.*, 100, 3355
- Lin, J., Soon, W., & Baliunas, S. L. 2003, *New Astro. Rev.*, 47, 53
- Lin, J. 2004, *Sol. Phys.*, 221, 115
- Lin, J., Ko, Y.-K., Sui, L., et al. 2005, *ApJ*, 622, 1251
- Liu, W., Jiang, Y. W., Liu, S., & Petrosian, V. 2004, *ApJ*, 611, L53
- Livi, S. H., Martin, S., Wang, H. M., & Ai, G. X. 1989, *Sol. Phys.*, 121, 197L
- Magara, T., & Shibata, K. 1999, *ASSL*, 240, 341
- Martens, P. C. H. 2003, *Adv. Space Res.*, 32, 905
- Martin, S. F. 1989, *Sol. Phys.*, 121, 215
- Masuda, S., Kosugi, T., Hara, H., Tsuneta, S., & Ogawara, Y. 1994, *Nature*, 371, 495
- McKenzie, D. E., & Hudson, H. S. 1999, *ApJ*, 519, L93
- Miyagoshi, T., Yokoyama, T., Shimojo, M. 2004, *PASJ*, 56, 207
- Moore, R. L. 1976, *BAAS*, 8, 549
- Moore, R. L., McKenzie, D. L., Švestka, Z., et al. 1980, In: Sturrock, P.A.(Ed.), *Solar Flares*.  
Colorado Assoc. Univ. Press, Boulder, pp. 341-409
- Moore, R. L., Hurford, G. J., Jones, H. P., & Kane, S. R. 1984, *Sol. Phys.*, 276, 379

- Moore, R. L., & Roumeliotis, G. 1992, in IAU Collq. 133, Eruptive Solar Flares, ed. Z. Švestka, B. V. Jackson, & M. E. Machado (New York: Springer), 69
- Moore, R. L., Sterling, A. C., Hudson, H. S., & Lemen, J. M. 2001, ApJ, 552, 833
- Ogawara, Y., Takano, T., & Kato, T. 1991, Sol. Phys., 136, 1
- Ohyama, M., & Shibata, K., 1997, PASJ, 49, 249
- Ohyama, M., & Shibata, K., 1998, ApJ, 499, 934
- Patterson, A., & Zirin, H. 1981, ApJ, 243, L99
- Pneuman, G. W. 1981, in Solar Flare Magnetohydrodynamics, ed. E.R. Priest (New York: Gordon & Breach), 379
- Priest, E., & Forbes, T. 1990, Sol. Phys., 126, 319
- Priest, E. R., & Forbes, T. G. 2000, Magnetic Reconnection: MHD Theory and Applications (Cambridge: Cambridge Univ. press)
- Priest, E. R., & Forbes, T. G. 2002, A&AR, 10, 313
- Qiu, J., Lee, J., Gary, D. E., & Wang, H. 2002, ApJ, 565, 1335
- Qiu, J., Lee, J., & Gary, D. E. 2004, ApJ, 603, 335
- Rust, D. M. 1972, Sol. Phys., 25, 141
- Scherrer, P. H., Bogart, R. S., Bush, R. I., et al. 1995, Sol. Phys., 162, 129
- Shibata, K., Masuda, S., Shimojo, M., Hara, H., Yokoyama, T., Tsuneta, S., Kosugi, T., & Ogawara, Y. 1995, ApJ, 451,L83
- Shibata, K. 1999, Ap&SS, 264, 129
- Shiota, D., Isobe, H., & Chen, P. F. 2005, ApJ, 634, 663
- Siarkowski, M., & Falewicz, R. 2004, A&A, 428, 219
- Sterling, A. C., Hudson, H. S., Thompson, B. J., & Zarro, D. M. 2000, ApJ, 532, 628
- Sterling, A. C., & Moore, R. L. 2005, ApJ, 630, 1148
- Sturrock, P. A. 1966, Nature, 211, 695

- Su, Y. N., Golub, L., & Van Ballegooijen, A. A. 2007, *ApJ*, 655, 606
- Svestka, Z., Farnik, F., Hick, P., Hudson, H. S., & Uchida, Y. 1997, *Sol. Phys.*, 276, 355
- Tajima, T., & Shibata, K. 1997, *Plasma Astrophysics* (Reading: AddisonWesley)
- Takakura, T., Tsuneta, S., Nitta, N., & Ohki, K. 1983, *Sol. Phys.*, 86, 323
- Temmer, M., Veronig, A. M., Vršnak, B., & Miklenic, C. 2007, *ApJ*, 654, 665
- Tian, L. R., & Alexander, D. 2006, *Sol. Phys.*, 233, 29
- Tripathi, D., Bothmer, V., & Cremades, H. 2004, *A&A*, 422, 337
- Tripathi, D. 2005, Ph.D. Thesis University of Göttingen, Copernicus GMBH
- Tripathi, D., Isobe, H., & Mason, H. E. 2006a, *A&A*, 453, 1111
- Tripathi, D. 2006b, *JA&A*, 27, 193
- Tsuneta, S., Acton, L., Bruner, M., et al. 1991, *Sol. Phys.*, 136, 37
- Tsuneta, S., Hara, H., Shimizu, T., et al., 1992, *PASJ*, 44, L63
- Valori, G., Kliem, B., & Keppens, R. 2005, *A&A*, 433, 335
- Wang, H. M., Qiu, J., Jing, J., et al. 2004, *ApJ*, 605, 931
- Wang, H. M., Song, H., Jing, J., et al. 2006, *Chin. J. Astron. Astrophys.*, 6, 477
- Wang, H. N., Yan, Y. H., & Sakurai, T. 2001, *Sol. Phys.*, 201, 323
- Wang, J. X., & Shi, Z. X. 1992, *Sol. Phys.*, 140, 67
- Wang, J. X., & Shi, Z. X. 1993, *Sol. Phys.*, 143, 119
- Webb, D. F., & Hundhausen, A. J. 1987, *Sol. Phys.*, 108, 383
- Wiegelmann, T., Lagg, A., Solanki, S., Inhester, B., & Woch, J. 2005, *A&A*, 433, 701
- Winglee, R. M., Dulk, G. A., Bornmann, P. L., & Brown, J. C. 1991, *ApJ*, 375, 382
- Wu, S. T., Wu, C. C., & Dryer, M. 1992, *ESASP*, 346, 333
- Yan, Y. H., & Wang, J. X. 1995, *A&A*, 298, 277
- Yokoyama, T., & Shibata, K. 1998, *ApJ*, 494, L113



- Yokoyama, T., & Shibata, K. 2001, ApJ, 549, 1160
- Zhang, J., Wang, J. X., Deng, Y. Y., & Wu, D. J. 2001a, ApJ, 548, L99
- Zhang, J., Wang, J. X., & Nitta, N. 2001b, Chin. J. Astron. Astrophys., 1, 85
- Zhang, J., & Wang, J. X. 2002, ApJ, 566, L117
- Zhang, J., Li, L. P., & Song, Q. 2007, ApJ, 662, L35
- Zhang, Y. Z., Wang, J. X., Hu, Y. Q. 2006, ApJ, 641, 572
- Zhao, H., Wang, J. X., Zhang, J., Xiao, C. J., & Wang, H. N. 2007, Chin. J. Astron. Astrophys., in press

Table 1. The information of the events

Date	PT(UT)	FC	Dur(min)	Len(Mm)	Vp(km/s)	ap(m/s <sup>2</sup> )	Vs(km/s)	Pos
14-Jul-98	12:59	M4.6	12	46.4	19.6	10.5	5.9	S23E20
23-Aug-98	09:34	M2.2	24	39.5	31	-11	7.5	N32E33
23-Sep-98	07:13	M7.1	51	80	38.7	-20.3	11.7	N18E09
30-Sep-98	13:40	M2.8	100	...	26.7	-94.4	...	N23W81
05-Nov-98	19:55	M8.4	72	35.7	27.2	76.5	13.2	N18W21
30-Dec-98	05:46	M1.0	34	71.2	4.6,4.5,5.7	-0.3	8	N28E03
18-Jan-99	08:04	M2.0	31	...	13.8	-8.3	...	N19E03
28-Feb-99	16:39	M6.6	12	90	21.4	-93.1	11.6	N28W06
10-May-99	05:31	M2.5	15	57.8	25	-43	8.8	N14E02
22-Jun-99	18:29	M1.7	77	...	17.8,17	-1.8	...	N25E40
02-Jul-99	01:38	M2.5	18	44.9	11.1	-2.8	...	S27E05
05-Jul-99	18:48	M1.2	36	34.2	10.9	2.8	1.2	S25W43
25-Jul-99	13:38	M2.4	69	49	31	-36	...	N38W81
20-Oct-99	06:22	M1.7	50	71	23.4,19.4	-17.3	11.8	N10W48
26-Oct-99	18:52	M2.3	22	50	13.8,12.1	-66.2	6.1	S13W02
12-Nov-99	09:16	M1.7	42	105	26	-4.6	3.6	N10E05
12-Nov-99	11:54	M1.1	7	55	17.6	-3.8	...	N10E17
16-Nov-99	14:11	M1.4	49	...	6.4,3	-5.6	...	S09E06
22-Jan-00	18:01	M1.0	12	34	18.8	-35	9.1	S23W50
08-Feb-00	09:00	M1.3	36	114	33.4,13.8	45.7	14.9	N25E26
24-Mar-00	07:52	X1.8	18	71.3	26.9	13.7	...	N16W82
11-Apr-00	18:10	M1.0	20	...	16.5	27.1	...	S16W18
12-Apr-00	03:35	M1.3	23	...	8.9	-8.7	...	S15W24
19-May-00	00:58	M1.1	13	80	18.9	-27.6	3.8	N11E07
04-Jun-00	14:01	M3.2	14	70	17.4	-124.2	6.6	N20E35
06-Jun-00	14:01	M7.1	15	89	22.2	-121	3.3	N19E14
06-Jun-00	15:25	X2.3	42	108.8	41.4	-166	9.3	N19E14
10-Jun-00	17:02	M5.2	39	92.6	48.9	34.4	13.6	N22W38
23-Jun-00	04:07	M2.6	12	45.3	16.5	-17	9.8	N19W30
25-Jun-00	07:52	M1.9	64	94.5	20.6,18.6	-3.9	3.7	N16W55
10-Jul-00	20:05	M1.9	18	31.3	14.4	3.1	3.7	N16W43
11-Jul-00	13:10	X1.0	83	111.2	11.9	7.9	...	N18E45
12-Jul-00	05:02	M1.2	14	68.2	10.1,8.9,4.2	4.7	5.3	N16E31
12-Jul-00	18:49	M5.7	26	90.1	17.2,2.9	-27.1	9	N16W64
14-Jul-00	10:24	X5.7	40	204	58.3,30.5	-134.7	23.6	N22W07
14-Jul-00	13:52	M3.7	16	63.5	15.8	-39.1	5.9	N20W08
17-Jul-00	00:34	M1.4	38	39	5.3,2.5	-3.6	9.7	N09E81
18-Jul-00	05:15	M1.9	39	82	19.8	1.4	3.8	N17W58
25-Jul-00	18:46	M1.2	16	33.9	30.5	-48.8	5.6	N05W16
25-Sep-00	02:15	M1.8	20	...	16.2,11.5	-7.9	...	N15W42
21-Oct-00	18:31	M3.0	33	...	8.8,8.8	-5.1	...	N17E23
08-Nov-00	23:28	M7.4	83	...	4.8,4.4	-0.3	...	N05W75
24-Nov-00	15:13	X2.3	30	66	...	...	12.9	N22W07
24-Nov-00	21:59	X1.8	29	54	...	...	14.3	N21W14
20-Mar-01	02:18	M1.1	19	62.8	14.8	-6.1	6.8	S05W54
20-Mar-01	15:07	M1.6	17	29.7	10.2	16.5	3.6	S05W61

Table 1—Continued

Date	PT(UT)	FC	Dur(min)	Len(Mm)	Vp(km/s)	ap(m/s <sup>2</sup> )	Vs(km/s)	Pos
21-Mar-01	02:37	M1.8	14	53.2	14.9	-25.8	...	S05W65
24-Mar-01	19:55	M1.7	72	40.4	32.5	-37	3.3	N15E22
28-Mar-01	12:40	M4.3	105	40.5	4.7,12.5	1.7	1.9	N18E02
29-Mar-01	14:58	M1.5	13	39.9	9.9	-13.6	...	N16W13
31-Mar-01	11:12	M2.1	31	50.5	18.7	0.1	3.7	N16W34
02-Apr-01	11:36	X1.1	67	68.1	13.7	-14.9	...	N11W91
03-Apr-01	23:51	M1.1	47	...	14.6	15	...	N16W88
09-Apr-01	15:34	M7.9	40	58.8	30.1	-32	3.3	S21W04
10-Apr-01	05:26	X2.3	36	141	49.2	-20.9	11.2	S23W09
11-Apr-01	13:26	M2.3	53	42.2	18.1,10.8	-21.8	5.4	S22W27
12-Apr-01	03:04	M1.3	33	33	18.5	-3.7	3.6	S22W38
12-Apr-01	10:28	X2.0	70	64.2	20.1	5.9	6.7	S19W43
19-Apr-01	11:35	M2.0	33	56	24.3	6.1	...	N14E60
20-Apr-01	05:23	M1.0	42	35.2	4.3,12.1	-3.8	6.2	N16E63
20-Apr-01	20:04	M4.1	25	...	33.6,19	-6.9	...	N15E55
23-Apr-01	01:28	M1.0	18	34.7	10.9	4	4.8	N18E18
23-Apr-01	20:30	M4.0	28	46.4	13.6	-2.5	...	N14E23
24-Apr-01	05:42	M2.1	14	...	19.8	-7.6	...	N18E01
24-Apr-01	22:24	M1.8	16	...	3.3	-11.8	...	N17E01
25-Apr-01	13:48	M2.7	20	...	8	-55.3	...	N18W09
26-Apr-01	13:12	M7.8	113	28.5	30.6	28.9	2.8	N17W31
27-Apr-01	19:15	M1.2	29	48	8.9	-7	...	N18W37
05-May-01	08:56	M1.0	33	52.5	5.3	-7.5	2.7	N25W06
12-May-01	23:35	M3.0	63	57.6	29.4	6.4	13.4	S17E00
13-May-01	03:04	M3.6	10	56.6	16.7	-14.4	10.6	S18W01
15-May-01	03:00	M1.0	15	66.3	19.7	-7.1	4.5	S17W29
04-Jun-01	22:59	M1.7	35	33.6	13.1,12.8	16.6	2.1	S05W04
15-Jun-01	10:13	M6.3	19	...	9.6	-5.3	...	S26E41
19-Jul-01	10:04	M1.8	25	54.9	19.1	-22.7	4.5	S08W62
05-Aug-01	22:24	M4.9	13	36.2	9.3,5.7,4.3	-6.2	4	S20W49
25-Aug-01	16:45	X5.3	41	118.9	33.4	14.3	16.3	S17E34
30-Aug-01	17:57	M1.5	26	27.9	3.4	-2.7	1.9	S21W28
02-Sep-01	13:48	M3.0	13	74.4	8.4	-12.9	...	S21W65
15-Sep-01	11:28	M1.5	50	...	13	-16.8	...	S21W49
28-Sep-01	10:14	M2.4	76	...	16.9	-0.2	...	S18W36
09-Oct-01	11:13	M1.4	63	...	17,27.4	12.2	...	S28E08
19-Oct-01	01:05	X1.6	26	...	30.8	-6.6	...	N16W18
19-Oct-01	02:32	M1.2	26	...	15.2	-18.3	...	N16W18
19-Oct-01	16:30	X1.6	30	...	18.5	-9.1	...	N15W29
23-Oct-01	02:23	M6.5	23	...	19	-16.5	...	S18E11
25-Oct-01	15:02	X1.3	46	...	17.8	1.9	...	S16W21
31-Oct-01	08:09	M3.2	45	...	11.8	-2.9	...	N11E02
01-Nov-01	23:52	M1.1	141	...	8.9,11.9	-2.6	...	N12W23
13-Dec-01	14:30	X6.2	15	70	...	...	29.9	N16E09
22-Feb-02	00:10	M4.4	38	...	8.4	-0.01	...	S20W20
14-Mar-02	01:50	M5.7	24	...	14.4,11.1	1.1	...	S12E23

Table 1—Continued

Date	PT(UT)	FC	Dur(min)	Len(Mm)	Vp(km/s)	ap(m/s <sup>2</sup> )	Vs(km/s)	Pos
15-Mar-02	23:10	M2.2	153	...	5.8	1.8	...	S08W03
18-Mar-02	02:31	M1.0	27	...	4.4,6.1	0.9	...	S09W47
09-Apr-02	13:02	M1.1	16	...	13.3	-25.8	...	N18E32
10-Apr-02	19:07	M1.6	27	...	26.8	-58.3	...	N20E31
16-Apr-02	13:19	M2.5	37	...	8.6	-20.9	...	N19W79
21-Apr-02	01:51	X1.5	115	...	18.8	0.4	...	S14W84
24-Apr-02	21:56	M1.7	15	...	12.5	-9.6	...	N09W49
30-May-02	17:24	M1.6	28	...	2.9	-4.7	...	S16E49
01-Jun-02	03:57	M1.5	11	...	7.1	-23.5	...	S19E29
02-Jul-02	20:31	M1.5	22	...	7.2,7.3	3	...	S18W46
29-Jul-02	02:38	M4.8	17	...	22.6	-21	...	S15W18
29-Jul-02	10:44	M4.7	46	72.1	7.8	3.5	4.5	S15W18
31-Jul-02	01:53	M1.2	23	53	29.9	-22.6	...	S13W30
03-Aug-02	19:07	X1.0	12	...	18.5	-19.3	...	X16W76
16-Aug-02	12:32	M5.2	95	88.5	12.1	-5.9	3.6	S14E20
16-Aug-02	22:12	M1.2	8	...	6.3	-5.1	...	S14E20
16-Aug-02	23:33	M1.7	6	...	4.9	-1.1	...	S05E06
17-Aug-02	01:08	M1.1	16	...	3.1	2.8	...	S19E77
17-Aug-02	20:51	M3.4	18	...	9.1	-13.2	...	S06W05
18-Aug-02	10:05	M2.3	15	...	12.2	19.2	...	S07W12
18-Aug-02	14:39	M1.9	10	...	2.7	-15.4	...	S06W15
18-Aug-02	21:25	M2.2	25	...	13.8	-11.9	...	S12W19
20-Aug-02	02:57	M1.4	8	...	9.7	7.8	...	S10W36
22-Aug-02	01:57	M5.4	18	...	19	10.4	...	S07W62
24-Aug-02	01:12	X3.1	42	...	36.1	15.5	...	S02W81
29-Sep-02	06:39	M2.6	9	...	7.1	2.8	...	N12E21
15-Oct-02	14:22	M1.0	29	...	18,14.2	-27.6	...	N20W04
22-Oct-02	15:35	M1.0	23	...	27.1	-85.3	...	N28E27
25-Oct-02	17:47	M1.5	59	...	22.4,22.2	-6.1	...	N28W11
28-Oct-02	12:05	M1.7	11	...	6.9	-17.3	...	N23W61
22-Jan-03	04:44	M1.2	15	...	13.3,7.5	-20.8	...	N15W05
19-Mar-03	03:07	M1.5	83	72.1	18	-25.4	1.2	S16W66
27-May-03	23:07	X1.3	17	42.2	...	...	12.3	S07W17
29-May-03	01:05	X1.2	21	34.6	16.5	-9.6	4.2	S06W37
31-May-03	02:24	M9.3	27	...	21	-25.6	...	S07W65
06-Jun-03	23:38	M1.0	27	...	9.2	-5.6	...	N13E17
11-Jun-03	00:02	X1.3	53	94.4	22.8,7.8	-0.6	4	N10W40
11-Jun-03	20:14	X1.6	26	77	18.8	-29	7.4	N14W57
17-Jun-03	22:55	M6.8	45	42.5	27.8	-10.5	...	S07E55
10-Jul-03	14:12	M3.6	29	...	23.7	-38	...	N12W82
16-Sep-03	22:24	M1.3	121	...	11.2	-0.6	...	S12W83
22-Oct-03	08:44	M1.7	23	42.5	6	8.2	...	N07E25
23-Oct-03	20:04	X1.1	24	56.6	25	-34.4	9.3	S17E84
24-Oct-03	02:54	M7.6	47	51	11.6	0.1	...	S19E72
26-Oct-03	06:54	X1.2	96	147.5	14.1	-5	4.4	S15E43
28-Oct-03	11:10	X17	93	147.6	36	-30.6	20.2	S16E26

Table 1—Continued

Date	PT(UT)	FC	Dur(min)	Len(Mm)	Vp(km/s)	ap(m/s <sup>2</sup> )	Vs(km/s)	Pos
29-Oct-03	20:49	X10	24	122	31.7	-22.9	26.7	S15W02
01-Dec-03	22:38	M3.2	23	44.5	10.2	-4.7	8.4	S12W60
04-Dec-03	19:50	X28	37	180.5	42.8	-16	...	S19W83
17-Dec-03	09:05	M4.2	24	50.8	14	-2.4	6.4	S01E33
18-Dec-03	07:52	M3.2	43	64.3	10	-23.8	4.8	N00E18
18-Dec-03	08:31	M3.9	47	97.1	...	...	14.4	N00E18
18-Dec-03	10:11	M4.5	98	88.6	5.6	-1.1	0.7	N00E08
05-Jan-04	03:45	M6.9	150	65	...	...	1.6	S10E24
26-Feb-04	02:03	X1.1	20	...	15.9	14.2	-29.4	N14W15
26-Feb-04	22:30	M5.7	25	54.3	5.8	-9.5	1.7	N14W26
06-Apr-04	13:28	M2.4	76	86.1	27.8	5.2	2.8	S18E15
13-Jul-04	00:17	M6.7	14	35.2	16	-12.4	12.6	N15W49
13-Jul-04	08:48	M5.4	15	55	2.9	-17.1	8.3	N12W52
13-Jul-04	19:32	M6.2	12	37.4	11.3	-6.7	7.2	N13W56
14-Jul-04	05:23	M6.2	25	42.9	...	...	4.8	N12W62
15-Jul-04	18:24	X1.6	13	46.5	19	-47.6	6.3	S11E56
16-Jul-04	02:06	X1.3	29	35.6	23.4	-35.2	7	S10E36
18-Jul-04	02:57	M1.5	12	37.2	7.4	0.8	4.2	S12E12
20-Jul-04	12:32	M8.6	23	75.7	19.5	-26.3	10.5	N11E34
25-Jul-04	05:51	M7.1	19	41.5	12.5	-19.4	12.8	N10W31
27-Jul-04	00:00	M1.2	25	66	7.9,7.4	-10.9	2.8	N10W54
18-Aug-04	17:40	X1.8	25	73	21	16.4	...	S12W83
31-Aug-04	05:38	M1.4	23	61.2	32.8	47.3	...	N04W87
12-Sep-04	00:56	M4.8	89	55.9	25.8,13.1	-28.2	3.5	N04E42
14-Sep-04	09:30	M1.5	133	57.6	11.8,6.4	-5	4	N04E17
15-Jan-05	23:02	X2.6	66	118.8	32.8	-15	9.3	N14W09
20-Jan-05	07:01	X7.1	50	102.1	29.5	-9.5	6.6	N12W58
06-May-05	11:28	M1.3	24	...	19.3	2.5	...	S04W76
17-May-05	02:39	M1.8	21	42.4	22.7,7.2	-6.4	1	S15W00
03-Jun-05	04:11	M1.3	13	31.9	12.4	-35	...	S17E22
16-Jun-05	20:22	M4.0	41	...	20	-17	...	N08W90
09-Jul-05	22:06	M2.8	32	94.4	17	-47.7	5.4	N12W28
27-Jul-05	05:02	M3.7	57	60.8	21.5	-16.2	...	N11E90
30-Jul-05	06:35	X1.3	44	...	51.5,39.5	14.8	...	N12E60
31-Jul-05	12:24	M1.1	18	32.2	16.8	-4.4	0.7	N13E45
01-Aug-05	13:51	M1.0	89	49.9	9.8	1.7	3.8	N13E32
08-Sep-05	21:06	X5.4	25	145.3	30.7	5.7	...	S12E75
09-Sep-05	05:03	M1.8	26	66.5	8.9	1.2	1.1	S12E68
09-Sep-05	05:48	M6.2	28	99	20.6	-0.1	...	S23E71
09-Sep-05	20:04	X6.2	83	227.6	19.7	-1.1	6.6	S12E67
11-Sep-05	02:35	M3.4	11	...	8.9	-3.8	...	S12E41
11-Sep-05	13:12	M3.0	69	42.5	6.6	-1	1.3	S13E41
13-Sep-05	19:27	X1.5	98	166.7	28.4	-12	8	S11E17
16-Sep-05	17:48	M1.3	35	111.9	7.6	-10.6	2.6	S11W36
17-Sep-05	06:05	M9.8	17	81.1	20	-22.7	3.2	S11W51
02-Dec-05	10:12	M7.8	20	...	15.7	-35.3	...	S04E13

Table 1—Continued

Date	PT(UT)	FC	Dur(min)	Len(Mm)	Vp(km/s)	ap(m/s <sup>2</sup> )	Vs(km/s)	Pos
02-Dec-05	21:19	M2.0	40	...	3.8	-0.5	...	S02E08
27-Apr-06	15:52	M7.9	36	70.5	13.5,11	-12.9	2.6	S08E26
06-Jul-06	08:36	M2.5	38	100.5	36	40.5	7.2	S09W34
06-Dec-06	18:47	X6.5	31	105.1	24.7	-11.6	16.3	S05E64
13-Dec-06	02:40	X3.4	43	162.7	31.4	-16.6	10.5	S06W23
14-Dec-06	22:15	X1.5	79	97.9	14.4	-23.4	8.2	S06W46

Table 2. The 8 parameters and the corresponding flare events

	FC	FD	PD	Vp	ap	Len	SD	Vs
FC	190	190	183	183	183	124	101	101
FD		190	183	183	183	124	101	101
PD			183	183	183	117	94	94
Vp				183	183	117	94	94
ap					183	-	-	-
Len						124	101	101
SD							101	101
Vs								101

The number on the cross point of two parameters represents the flare events from which the corresponding two parameters are determined simultaneously.

Table 3. The information of the three types of propagation of the PFLs and the separation of the FRs.

Type	M-class	X-class	Total	Percentage	Vp(Vs)[km s <sup>-1</sup> ]	Standard Deviation[km s <sup>-1</sup> ]
I	76(50)	18(14)	94(64)	49.5%(51.6%)	18.3(8)	10.7(6.1)
II	41(23)	16(13)	57(36)	30%(29%)	16.8(6.3)	7.4(3.7)
III	34(20)	5(4)	39(24)	20.5%(19.4%)	17.7(6)	12.7(5)

The values in brackets, determined from TRACE 1600 Å observations, are relevant to the separation of the FRs. Otherwise the values are relevant to the propagation of the PFLs, derived from TRACE 171 Å observations.

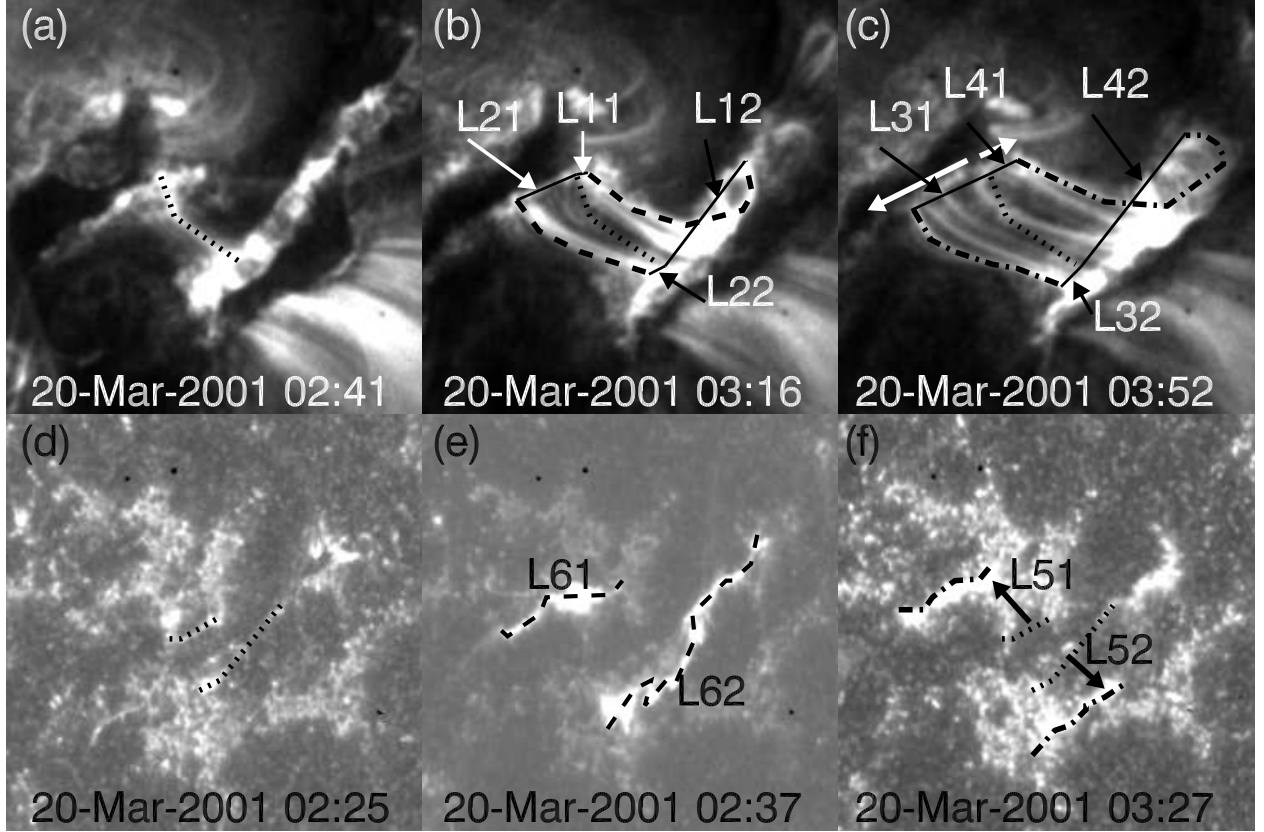


Fig. 1.— Time sequence of TRACE 171 Å (*a-c*) and 1600 Å (*d-f*) images showing a flare event on 2001 March 20. This event is employed to describe the method to measure the parameters relevant to the PFLs and the FRs (see the text). The dotted curves in (*a*)-(*c*) represent the initial brightening of the PFLs. The dashed curves in (*b*) and (*c*) outline the outer edges of the PFLs at 03:16 UT, and the dash dot curves in (*c*), the outer edges at 03:52 UT.  $L_1$  and  $L_2$  in (*c*) indicate the distance of the propagation of the PFLs from 02:41 UT to 03:52 UT towards southeast along the FRs, as well as  $L_3$  and  $L_4$ , towards northwest. The thick white arrows in (*c*) represent the propagating direction of the PFLs. The dotted curves in (*d*) and (*f*) represent the initial brightening of the FRs at 02:25 UT. The dash dot curves in (*f*) outline the outer edges of the FRs at 03:27 UT. The dashed curves in (*e*) mark the track of the FRs.  $L_{61}$  and  $L_{62}$  represent the length of the FRs.  $L_{51}$  and  $L_{52}$  in (*f*) are the average distance of the separation of the FRs from 02:25 UT to 03:27 UT. The black arrows in (*f*) point to the separating direction of the FRs. The field-of-view is  $125'' \times 125''$ .

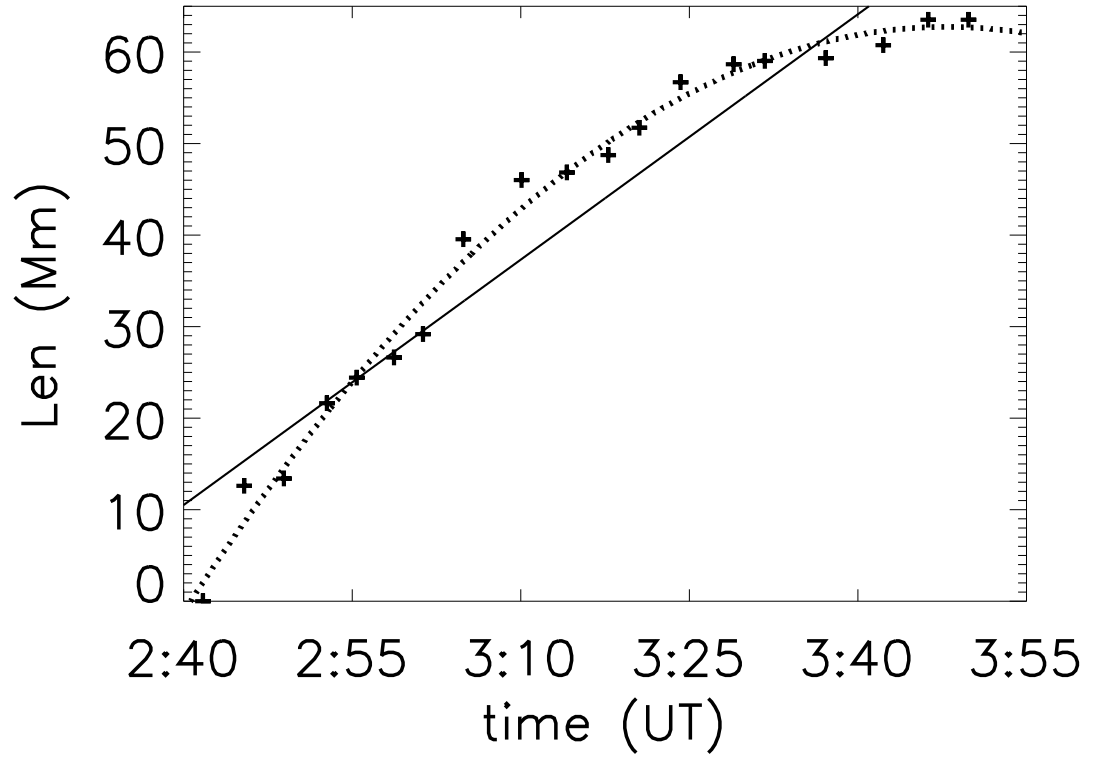


Fig. 2.— Distance versus time plot for the propagation of the brightening of PFLs for the event shown in Fig. 1. The solid line are linear fit to the data points, and the dotted line, second order polynomial fit.



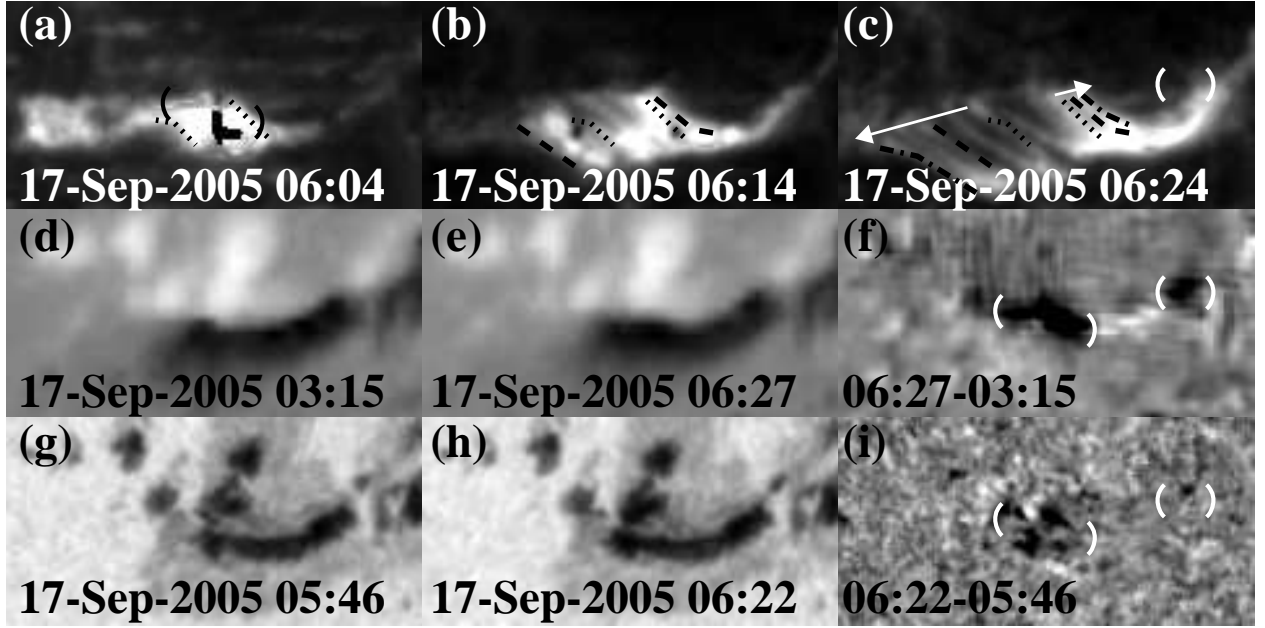


Fig. 3.— TRACE and SOHO/MDI observations showing a flare event on 2005 September 17. (a)-(c): time sequence of TRACE 171 Å images. (d)-(f): the observations of SOHO/MDI longitudinal magnetograms (*d* and *e*) and their difference image (*f*). (*g*) and (*i*): TRACE WL images (*g* and *h*) and their difference image (*i*). The curves and arrows represent the same signification as mentioned in Figs. 1a-1c. The brackets in (*f*) and (*i*) mark the regions where display distinct change of photospherical magnetic field and continuum intensity, and are overplotted on TRACE 171 Å images (a) and (c). The field-of-view is  $80'' \times 40''$ .

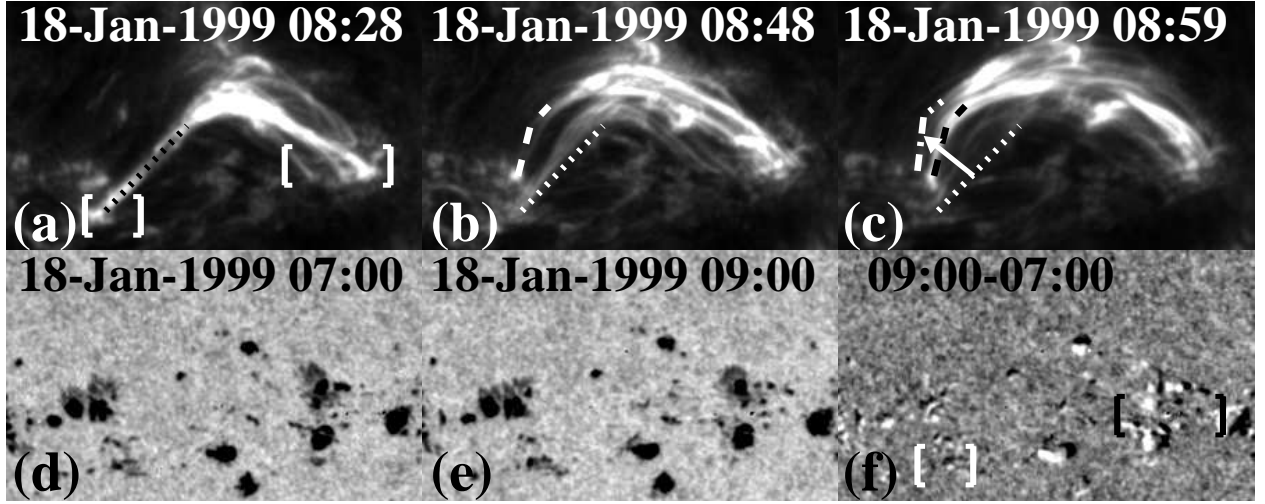


Fig. 4.— Similar to Fig. 3. TRACE observations showing a flare event on 1999 January 18. (a)-(c): time sequence of 171 Å images. (d)-(f): WL images (*d* and *e*) and their difference image (*f*). The curves, arrow and brackets denote the same meaning as in Fig. 2. The field-of-view is  $150'' \times 90''$ .

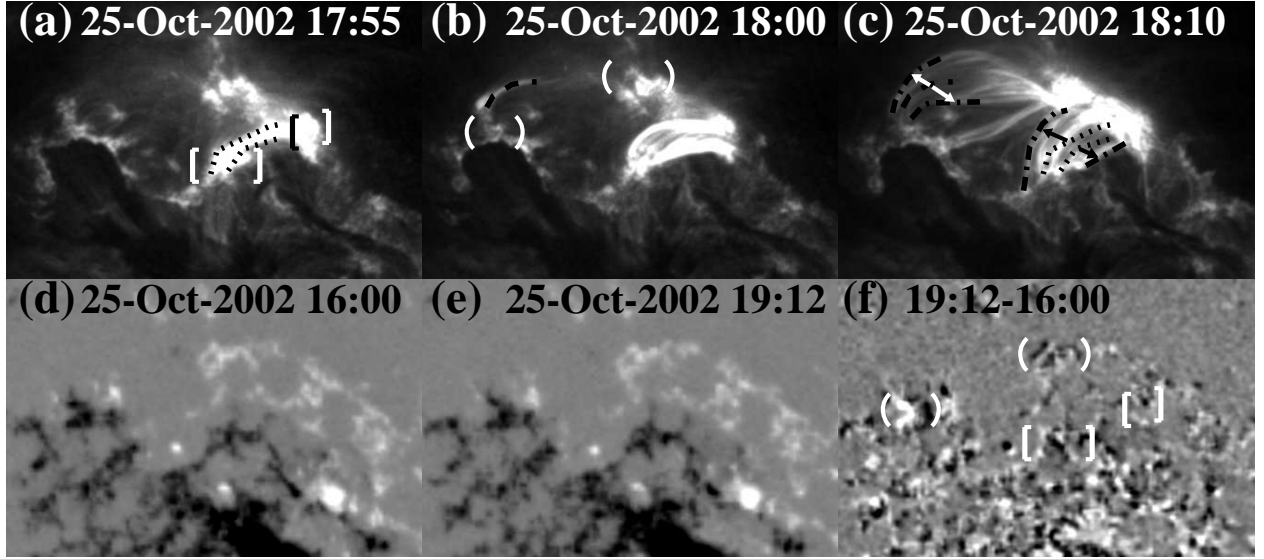


Fig. 5.— Similar to Fig. 3. TRACE and SOHO/MDI observations showing a flare event on 2002 October 25. (a)-(c): time sequence of TRACE 171 Å images. (d)-(f): the observations of SOHO/MDI longitudinal magnetograms (d and e) and their difference image (f). The dotted curves in (a) represent the outer edges of the initial brightening of a set of the PFLs in the southwest of the FRs at 17:55 UT, the dashed curve in (b), outlines the first brightening of another set of the PFLs in the northeast at 18:00 UT, the dash dot curves in (c), the outer edges of the two set of the PFLs at 18:10 UT. Black and white arrows in (c) represent the propagating direction of the brightening. The square brackets in (a) represent the region where displays the initial brightening in southwest of the FRs, and are overplotted on the difference magnetogram (f). The brackets in (b) and (f), the region in northeast. The field-of-view is  $225'' \times 150''$ .

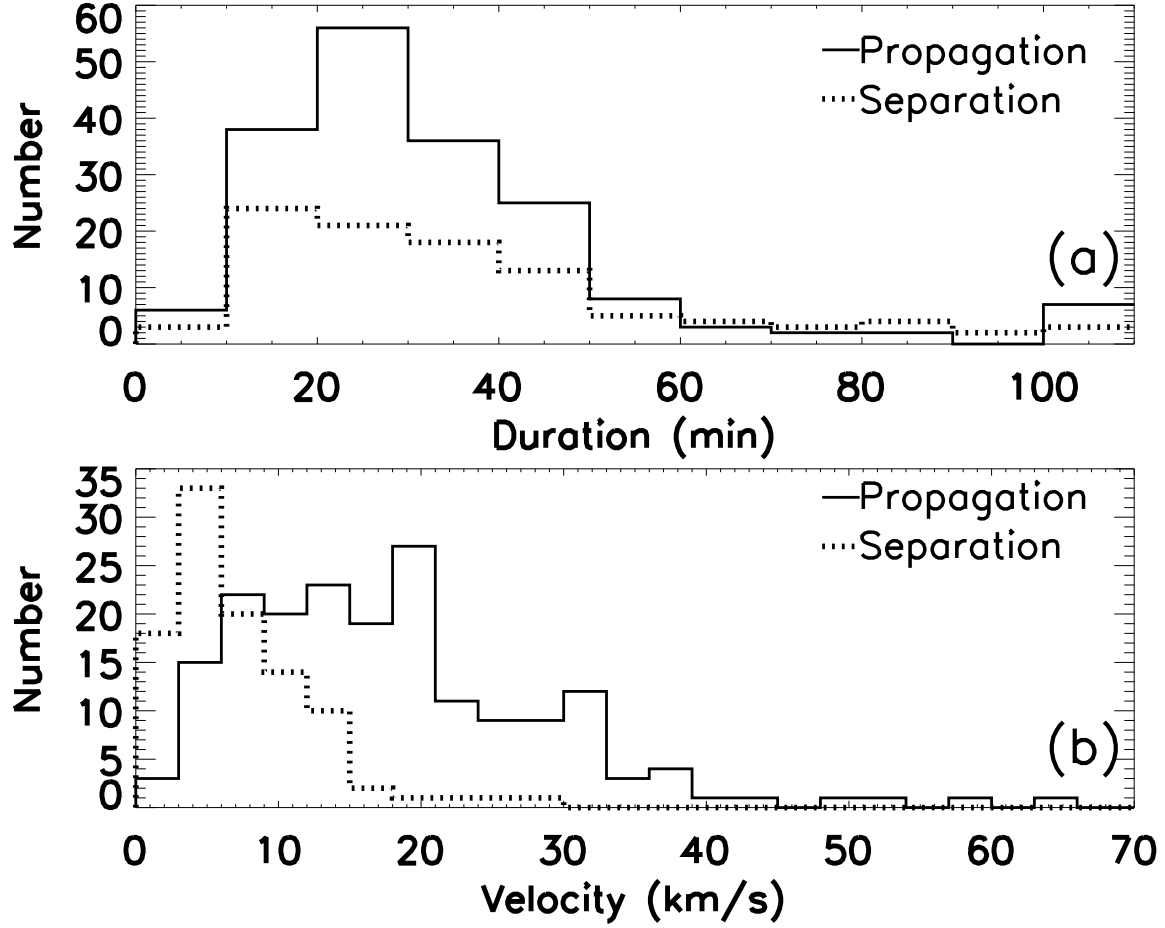


Fig. 6.— (a): histogram showing the distribution of  $PD$  (solid lines) and  $SD$  (dotted lines). (b): histogram displaying the distribution of  $V_p$  (solid lines) and  $V_s$  (dotted lines).

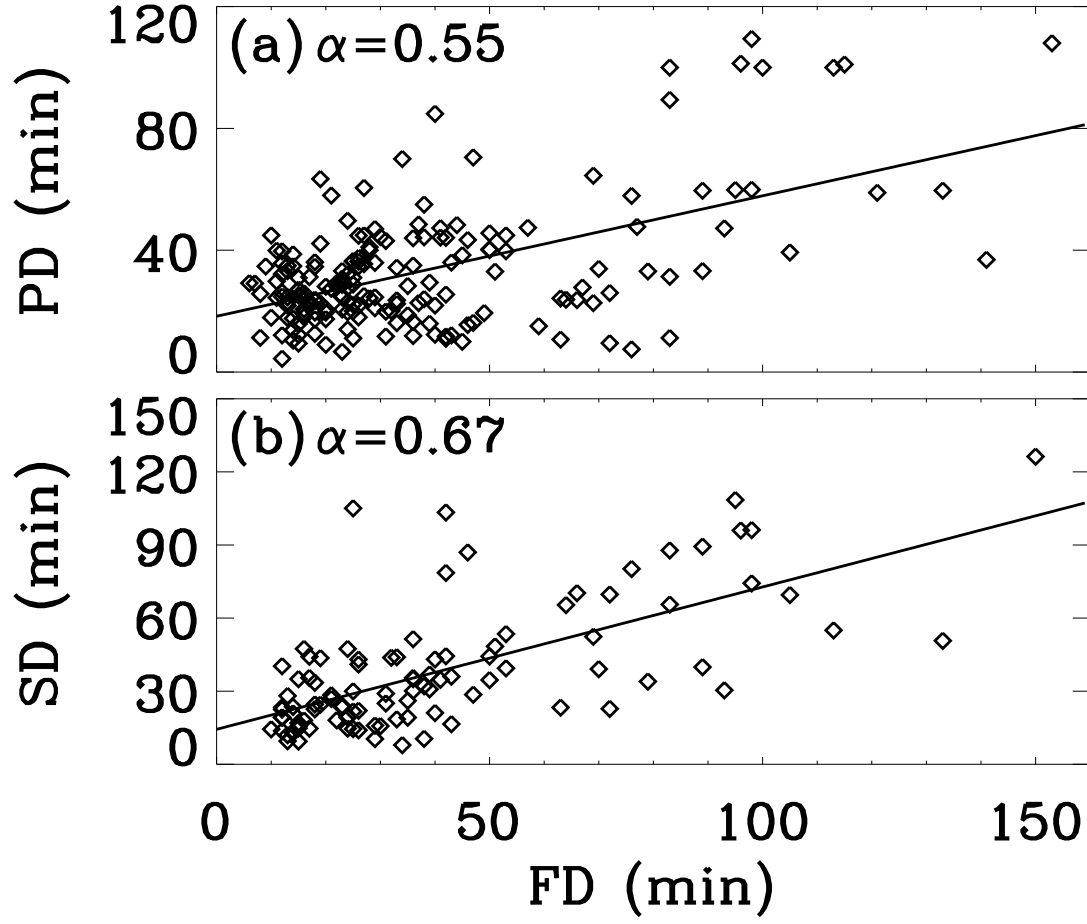


Fig. 7.— The relationships between  $PD$  and  $FD$  (a), as well as  $SD$  and  $FD$  (b).  $\alpha$  represents the correlation coefficient, and lines show the linear fitting of the data points.

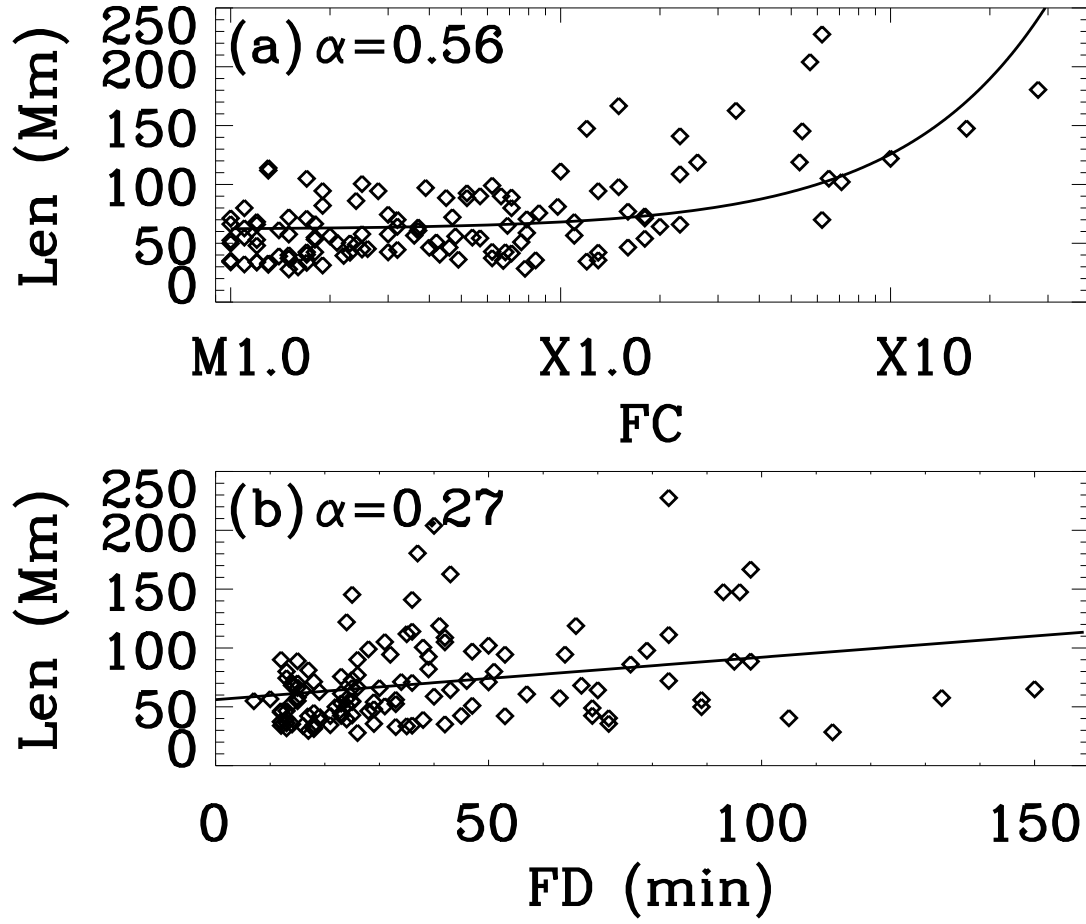


Fig. 8.— Same as Fig. 7, but for the relationships between  $Len$  and  $FC$  (a), as well as  $Len$  and  $FD$  (b).

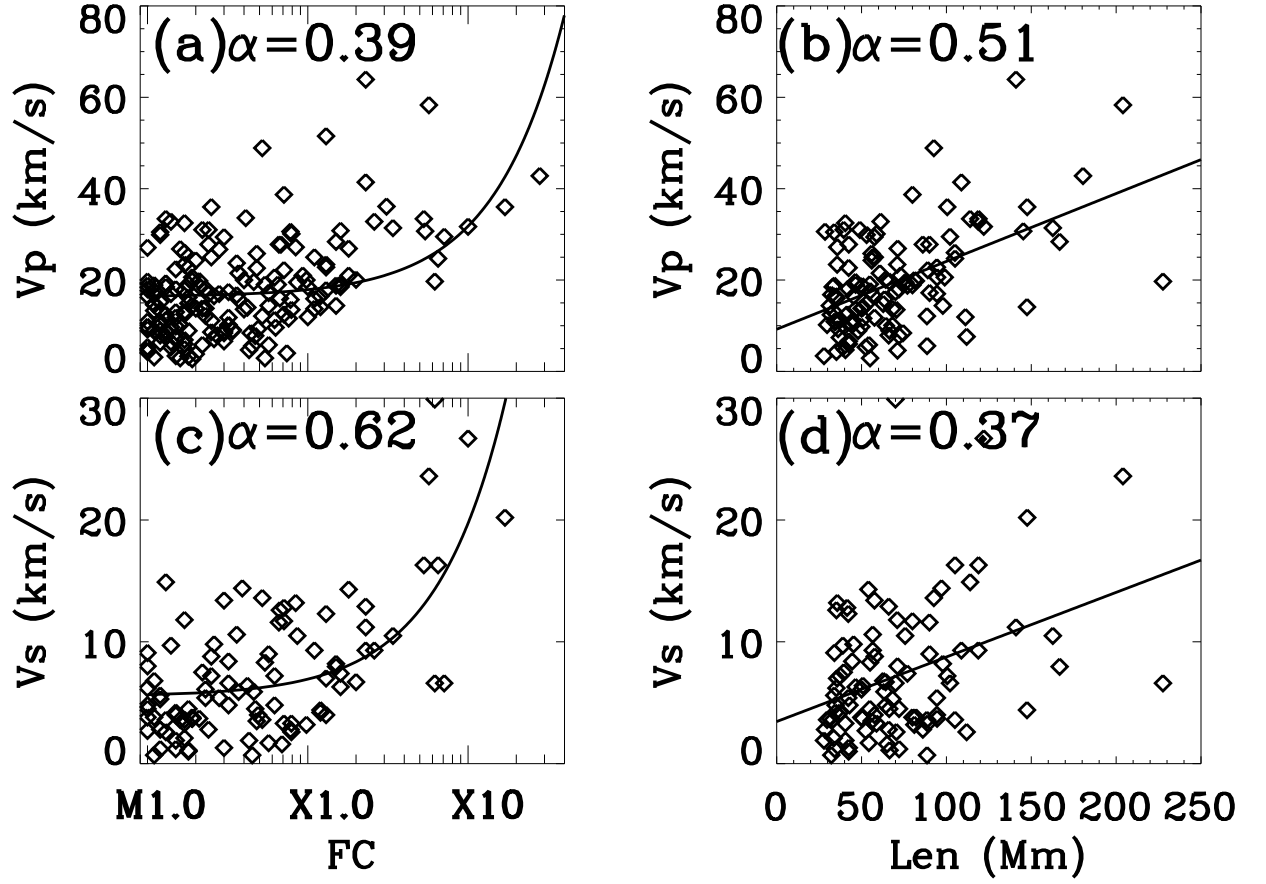


Fig. 9.— Same as Fig. 7, but for the relationships between  $V_p$  and  $FC$  (a),  $V_p$  and  $Len$  (b),  $V_s$  and  $FC$  (c), as well as  $V_s$  and  $Len$  (d).

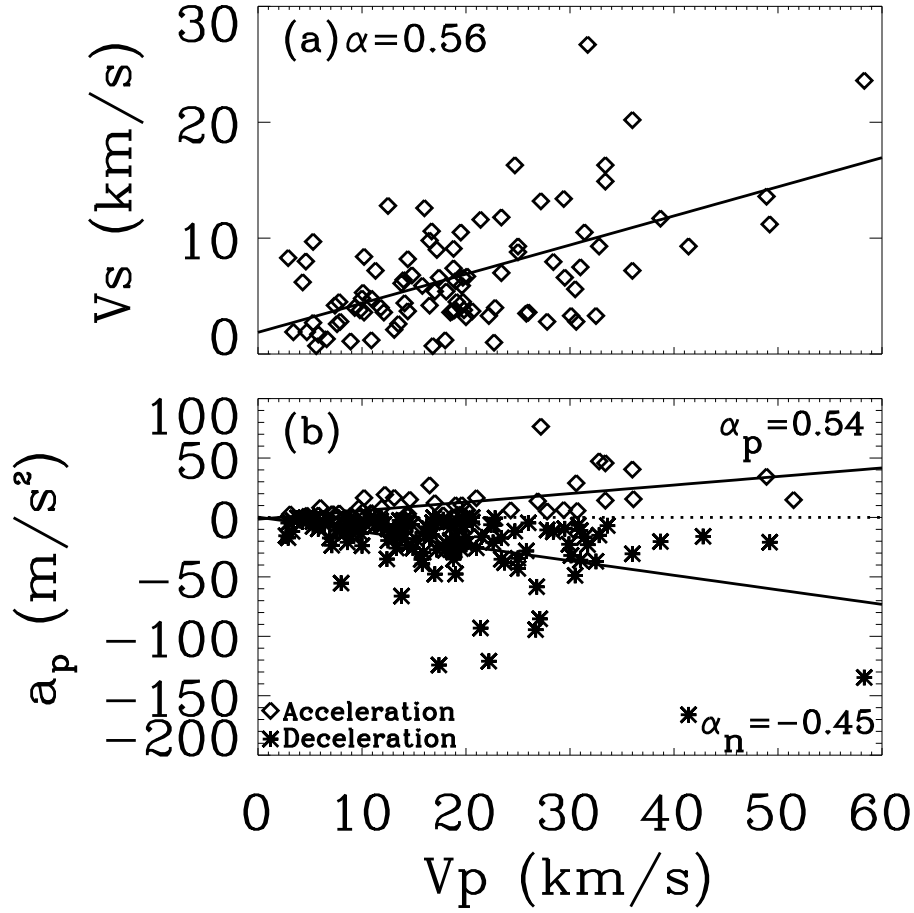


Fig. 10.— Same as Fig. 7, but for the relationships between  $V_s$  and  $V_p$  (a), as well as between  $a_p$  and  $V_p$  (b). The diamonds in (b) represent the events with positive acceleration, and the asterisks with negative acceleration.



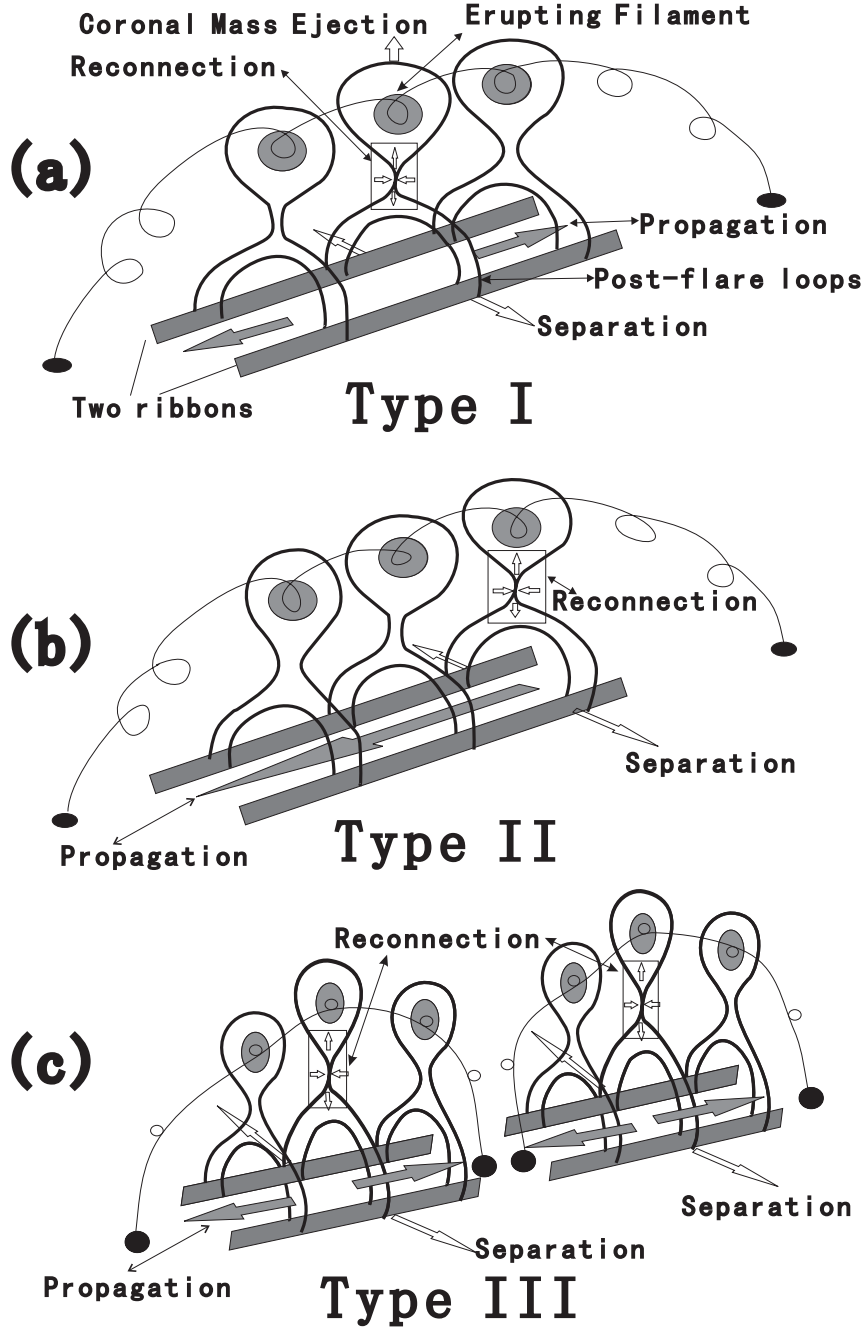


Fig. 11.— Schematic diagrams showing 3-dimensional magnetic reconnection in the process of flares and erupted filaments. These figures are taken from Shiota et al. (2005) and Tripathi et al. (2006a), and have been modified according to TRACE observations. For each figure, the thick curves show magnetic field lines, and the thin lines, magnetic flux ropes or filament. The gray thick lines mean the FRs. The region in the rectangle window represents the magnetic reconnection site. The arrows in this window means the moving direction of the material. The bigger grey arrows represent the propagation directions of the PFLs, and bigger hollow arrows the separating directions of the FRs.